discussion for a single geometry. The behavior reported here is quite universal in boundary lubrication by simple fluids. We have also studied different values of ϵ_{wf}, σ_{wf}, and normal load; different crystal faces and shear directions; solid walls with much higher density than the fluid; amorphous walls generated by the rapid quenching of a fluid state; and even the effect of introducing vacancies in the film. In each case, similar stick-slip behavior occurs. What changes are the values of f_s, f_m, and v_c, and the plate separation h_c at which stick-slip behavior starts. For example, we find that increasing the degree of corrugation in the wall-fluid potential increases f_m, v_c, and h_c.

When the walls are amorphous, the order induced in the fluid is no longer crystalline. Instead, a glassy structure that minimizes the wall-fluid interaction is observed. This leads to larger fluctuations in f_s, but the qualitative behavior is similar. Glassy states may also be formed by long-chain molecules between ordered plates because the relaxation of these molecules is slow (*8*). The interplay between molecular structure and ordering during stick-slip motion is an important issue for future work.

Another open question is whether stick-slip motion is caused by analogous mechanisms in other systems. The ordered static and disordered sliding states need not correspond to solid and fluid structure in an intermediate film. Instead, in the case of solid-on-solid sliding, they may correspond to states with and without chemical bonds or elastic deformations that increase the coupling between plates. For example, stick-slip motion of a weak solid over a hard solid leaves behind patches of the weak material (*1*), suggesting periodic welding of the surfaces followed by cracking. These and other possibilities remain to be explored.

REFERENCES AND NOTES

1. See, for example, F. P. Bowen and D. Tabor, *Friction and Lubrication* (Oxford Univ. Press, Oxford, 1958); E. Rabinowicz, *Friction and Wear of Materials* (Wiley, New York, 1965).
2. C. Scholz, P. Molnar, T. Johnson, *J. Geophys. Res.* 77, 6392 (1972).
3. J. N. Israelachvili, P. M. McGuiggan, A. M. Homola, *Science* **240**, 189 (1988); A. M. Homola, J. N. Israelachvili, M. L. Gee, P. M. McGuiggan, *J. Tribol.* **3**, 675 (1989).
4. P. M. McGuiggan, J. N. Israelachvili, M. L. Gee, A. M. Homola, *Mater. Res. Soc. Symp. Proc.* **140**, 79 (1989).
5. M. L. Gee, P. M. McGuiggan, J. N. Israelachvili, A. M. Homola, *J. Chem. Phys.* **93**, 1895 (1990).
6. P. A. Thompson and M. O. Robbins, *Phys. Rev. A* **41**, 6830 (1990).
7. R. Erlandsson, G. Hadziioannou, C. Mate, G. McClelland, S. Chiang, *J. Chem. Phys.* **89**, 5190 (1988).
8. J. Van Alsten and S. Granick, *Phys. Rev. Lett.* **61**, 2570 (1988); *Langmuir* **6**, 876 (1990); *Tribol. Trans.* **33**, 436 (1990).
9. M. Schoen, C. L. Rhykerd, Jr., D. J. Diestler, J. H. Cushman, *Science* **245**, 1223 (1989).
10. The simulations were performed in a constant number, load, and temperature ensemble. The number of fluid molecules N is not fixed in experiments. However, the time scale of stick-slip events is too short to allow significant transport from the bulk.
11. In the limit of infinitely stiff springs, the forward jump may reduce to a single lattice constant as seen in simulations of solid-on-solid sliding by U. Landman, W. D. Luedtke, and A. Nitzan [*Surf Sci.* **210**, L177 (1990)].
12. In particular, the shear plane in bulk films is very close ($<\sigma$) to the solid wall for $e^{-W} \sim 0.2$ (*6*).
13. B. J. Ackerson and N. A. Clark, *Phys. Rev. Lett.* **44**, 1005 (1980); *ibid* **46**, 123 (1981).
14. M. J. Stevens, M. O. Robbins, J. F. Belak, in preparation.
15. P. M. Chaikin, J. M. diMeglio, W. D. Dozier, H. M. Lindsay, D. A. Weitz, in *Physics of Complex and Supernolecular Fluids*, S. Safran and N. A. Clark, Eds. (Wiley-Interscience, New York, 1987), pp. 65–81.

16. We thank J. N. Israelachvili, P. M. McGuiggan, and M. J. Stevens for useful conversations. Supported through NSF grant DMR 85-53271 and allocations at the Pittsburgh Supercomputing Center. The work of M.O.R. was supported by the Sloan Foundation and through NSF grant PHY 82-17853 at the Institute for Theoretical Physics, where this project was conceived. The work of P.A.T. was supported by the Johns Hopkins University Applied Physics Laboratory.

8 May 1990; accepted 10 August 1990

Pressure Dependence of Elastic Wave Velocity for β-Mg_2SiO_4 and the Composition of the Earth's Mantle

GABRIEL D. GWANMESIA, SALLY RIGDEN, IAN JACKSON, ROBERT C. LIEBERMANN

The pressure dependence of the elastic wave velocities for hot-pressed, elastically isotropic polycrystals of the β (modified spinel) phase of magnesium orthosilicate (Mg_2SiO_4) has been determined at room temperature to 3 gigapascals (GPa) by ultrasonic pulse interferometry. Pressure derivatives of the bulk ($dK/dP = 4.8$) and shear ($dG/dP = 1.7$) moduli derived from the travel times of the compressional (P) and shear (S) waves clearly demonstrate that the velocity contrast between the olivine and β phases of Mg_2SiO_4 decreases with increasing pressure. When combined with plausible values for the (as yet unmeasured) temperature derivatives, these new data can be used to calculate the contrast in P and S wave velocities across an olivine–β phase transformation occurring at pressure-temperature conditions corresponding to about 400 kilometers depth in the earth. The seismologically observed contrasts ΔV in both P and S wave velocities constrain the percentage of orthosilicate in a model mantle of uniform chemical composition for appropriate relative magnitudes of the temperature (T) derivatives of the bulk and shear moduli for the β phase. Allowed combinations of orthosilicate content (percent), dK/dT, and dG/dT (both in gigapascals per Kelvin) for a pair of recent seismological models with $\Delta V_P = \Delta V_S = 4.6\%$ include (65, −0.018, −0.020), (55, −0.015, −0.018), and (45, −0.012, −0.016).

A CONTINUING CHALLENGE FOR Earth scientists has been to determine the relative contributions of isochemical phase transformation and chemical stratification to the discontinuous increases of seismic wave velocity with depth that characterize the transition zone (400 to 670 km depth) of the earth's mantle. A detailed knowledge of the chemical composition of the earth's mantle is vital in placing constraints on the early formation of the earth and on its thermal and chemical evolution.

Pioneering studies (*1*) suggested that phase transformations might play an important role in explaining the velocity and density structure of the transition zone. Subsequently it was demonstrated that the dominant minerals of the upper mantle (olivine and pyroxene) transform to more close-packed crystal structures under the pressure-temperature conditions of the transition zone (*2*) and that these transformations are likely to produce relatively sharp seismic discontinuities (*3*). In particular, the discontinuous increase in seismic wave velocity near 400 km depth has been attributed at least in part to the transformation of $(Mg,Fe)_2SiO_4$ olivine to the β phase (*4*).

More quantitative assessment of the nature of the 400-km discontinuity has been facilitated by measurements under ambient conditions of the elastic properties of single-crystal β-Mg_2SiO_4; these studies revealed that there is a ~13% contrast in elastic wave velocities between the olivine and β phases (*5, 6*). However, the conclusions of recent

G. D. Gwanmesia and R. C. Liebermann, Mineral Physics Institute and Department of Earth and Space Sciences, State University of New York at Stony Brook, Stony Brook, NY 11794.
S. Rigden and I. Jackson, Research School of Earth Sciences, Australian National University, Canberra, A.C.T., 2601, Australia.

analyses (7) of the composition of the transition zone, which involve extrapolation of these measurements to high pressure and temperature, are sensitive to the values assumed for the pressure and temperature derivatives of the elastic moduli. In this report we present measurements of the pressure dependence of the elastic wave velocities for β-Mg_2SiO_4 and use these results, along with plausible estimates of the corresponding temperature derivatives, to constrain the proportion of orthosilicate in the vicinity of the 400-km seismic discontinuity for an isochemical model mantle.

Samples of the high-pressure phases of Mg_2SiO_4 of moderate size can now be synthesized because of the development of large-volume high-pressure systems in Japanese laboratories. These systems are capable of simulating the conditions throughout the transition zone and into the uppermost part of the lower mantle while providing a uniform thermodynamic environment for the sample being synthesised. Dense isotropic polycrystals of the β phase of Mg_2SiO_4 have recently been successfully hot-pressed in a 2000-ton uniaxial split-sphere apparatus (USSA-2000) at pressures of 15 GPa and temperatures of 1000°C (*8*). Specimens were characterized by x-ray diffraction and by optical and electron microscopy.

Two cylindrical specimens (#786 and #897) (*8*) were chosen for ultrasonic characterization at high pressures. Elastic wave travel times were measured for P and S wave propagation along the cylindrical axis for each specimen and also normal to the cylindrical axis for sample #897 as a check on possible elastic anisotropy.

Elastic wave travel times were measured with the phase comparison method of ultrasonic pulse interferometry (*9*) at pressure in a liquid-medium piston-cylinder apparatus (*10, 11*). Access to a wide frequency range is a major advantage of this method for the characterization of relatively small specimens. Earlier studies of sintered polycrystals of standard materials have indicated that these methods yield pressure derivatives consistently within 10% of those calculated from the results of single-crystal studies (*11*).

The variation with pressure of the travel times for P and S waves was used to correct the velocities and associated elastic moduli for pressure-induced dimensional changes (*12*) (Fig. 1). For pressures greater than ~1.4 GPa (*13*), linear velocity-pressure trends are observed that extrapolate to velocities marginally higher than those measured at atmospheric pressure. These extrapolated velocities are depressed by 1.8% for P waves and 0.5% for S waves below the mean of the Hashin-Shtrikman bounds calculated

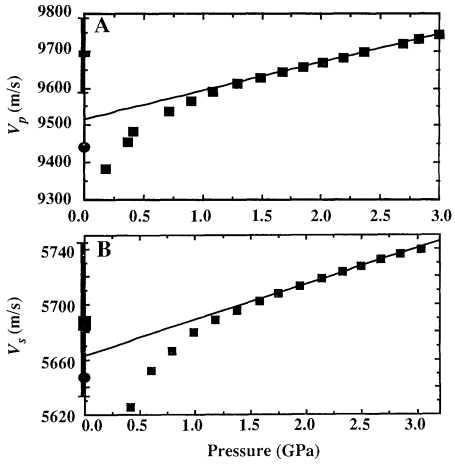

Fig. 1. Variation of elastic wave velocity with pressure for β-Mg_2SiO_4 specimen β786; squares are high-pressure data; circles indicate measurements at ambient pressure. For both compressional (**A**) and shear (**B**) waves, the high-pressure data extrapolate to values slightly greater than those measured at 1 atm. Rectangles show Hashin-Shtrikman bounds calculated from single-crystal elastic moduli (*5*) for an ideal, isotropic polycrystalline aggregate; error bars are ±1%.

from single-crystal elasticity data (*5*). However, within the mutual uncertainties associated with the ultrasonic (±0.25%) and Brillouin spectroscopic (±1%) techniques, these atmospheric pressure data are in good agreement.

In order to facilitate the consistent extrapolation of these results to the much higher pressures of the transition zone, the shear (G) and compressional ($Mp = K + 4G/3$, where K is the bulk modulus) moduli have been fitted to functions of the Eulerian strain $\varepsilon(\varepsilon = [1 - (\rho/\rho_0)^{2/3}]/2$, where ρ is the density) as follows:

$$G = (1 - 2\varepsilon)^{5/2}(M_1 + M_2\varepsilon) \quad (1)$$

$$Mp = (1 - 2\varepsilon)^{5/2}(L_1 + L_2\varepsilon) \quad (2)$$

The coefficients of these polynomials are related to the bulk and shear moduli and their pressure derivatives at zero pressure (dK/dP and dG/dP) (*14*).

Values of dK/dP and dG/dP obtained for the β phase in this way are given in Table 1. The preferred values of $dK/dP = 4.8$ and $dG/dT = 1.7$ are those from specimen β786. Those from specimen β897 demonstrate that the experiments are reproducible, even though the travel time–dispersion curves are more complicated for this specimen as a consequence of its smaller size and less regular shape. Moreover, the data from β897 in the z and x directions are identical, which clearly shows that these hot-pressed polycrystalline specimens are elastically isotropic, not only at atmospheric pressure (*8*), but also in the pressure dependence of their wave velocities. Also included in Table 1 are

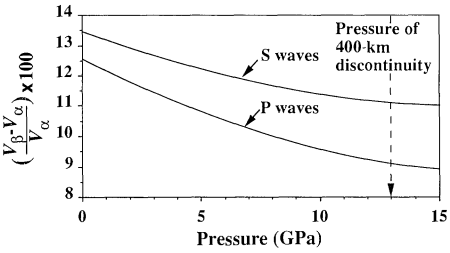

Fig. 2. Percentage change in velocity across the olivine (α) to β spinel phase transition in Mg_2SiO_4 for both P and S waves as a function of pressure at ambient temperature. In both cases pressure reduces the contrast, but the effect is more dramatic for P waves. At the pressure of the 400-km seismic discontinuity (dashed line), the contrast is ~9% for P waves and ~11% for S waves.

Table 1. Pressure derivatives of elastic moduli for the β and olivine phases of Mg_2SiO_4. Numbers in parentheses are estimated errors in last significant digit and include allowances for possible systematic errors in the experiments. The z direction (dir) is parallel to the cylindrical axis of the specimen; the x direction is perpendicular to the cylindrical axis.

Sample	dK/dP	dG/dP
β-Mg_2SiO_4		
β786	4.8(2)	1.7(1)
β897, z dir	4.7(2)	1.9(1)
β897, x dir	4.7(2)	1.9(1)
D&A*	4.9	1.8
Mg_2SiO_4 olivine†	5.4	1.8

*Estimate from (*16*). †From (*6*).

the predictions based on empirical systematics among the so-called {DLA} parameters (*15, 16*). In view of the scatter of the data about these trends, the pressure derivatives for the β phase were surprisingly well predicted.

The new data for the pressure dependence of the elastic moduli for the β phase provide a firmer basis for the discussion of the magnitude of the 400-km seismic discontinuity and the composition of the transition zone than has hitherto (*4–6, 15–18*) been possible. A number of recent upper mantle body wave studies indicate that the velocity contrast across the discontinuity near 400 km depth is 3.8 to 4.9% for P waves and 4 to 5% for S waves (*19*). There is thus no clear requirement that the velocity contrasts for P and S waves be different. Therefore we use the results from two recent models (*20*) with velocity contrasts of 4.6% for both P and S waves in our analysis. At ambient conditions, the olivine to β phase transformation results in an increase of ~13% in velocity for both P and S waves (Fig. 2). If the magnitude of this contrast were preserved at high pressure and temperature, then matching the size of the 400-km discontinuity would require ~35% orthosili-

cate in the mantle.

However, our experimental data demonstrate that the velocities of both P and S waves increase less rapidly with increasing pressure at ambient temperature for the β phase than for the olivine phase of Mg_2SiO_4. This results in a marked decrease in the velocity contrast between the two polymorphs at pressures corresponding to 400 km depth (Fig. 2) and a higher inferred orthosilicate content (42% for S waves, 51% for P waves) for the model mantle with $\Delta V_P = \Delta V_S = 4.6\%$.

For more complete analysis of this problem, the temperature derivatives of the elastic moduli are also required. Because these are yet to be measured and can probably not be estimated with sufficient precision, the approach we adopt is to determine plausible combinations of dK/dT, dG/dT, and orthosilicate content of the model mantle that provide a quantitative explanation of the magnitude of the observed discontinuity in seismic wave velocities near 400 km, under the assumption that this discontinuity is due solely to an isochemical transformation from olivine to the β phase.

In order to extrapolate to the conditions in the deep earth, we first correct densities and elastic moduli for composition and temperature at atmospheric pressure following the approach taken by Duffy and Anderson (*16*). The relevant temperature is the potential temperature [1300°C (*21*)] at the zero-pressure intercept of the appropriate mantle adiabat. Third-order Eulerian finite-strain adiabats are then constructed to project densities and elastic moduli, and hence wave velocities, to the pressures at depth.

The sparse measurements of dG/dT and dK/dT for mantle minerals and relevant close-packed oxides fall between the following bounds (in gigapascals per Kelvin): $-0.014 > dK/dT > -0.021$; $-0.010 > dG/dT > -0.024$ (*22*). The values of dK/dT and dG/dT required, along with the newly measured pressure derivatives, to yield a velocity contrast of 4.6% for both P and S waves across the 400-km discontinuity are indicated by the bold curve of Fig. 3. As the temperature derivatives increase in magnitude along this curve, the inferred orthosilicate content of the model mantle increases from ~40% to ~70% as indicated. Allowed combinations of orthosilicate content (in percent, dK/dT, dG/dT (in gigapascals per Kelvin) for $\Delta V_P = \Delta V_S = 4.6\%$ thus include (65%, −0.018, −0.020), (55%, −0.015, −0.018), and (45%, −0.012, −0.016).

The relatively minor displacements of this curve induced by changes of ±100°C in the potential temperature are shown by the vertical bars. However, the effect of perturbing the seismologically inferred relative velocity contrast (so that $\Delta V_P \neq \Delta V_S$) is far more dramatic. The filled circles on the bold curve are displaced along the broken lines by changes of ±0.5% in ΔV_P (that is, to 5.1 and 4.1%, respectively) at constant ΔV_S, and vice versa, at fixed orthosilicate content. In all cases a strong trade-off between the two temperature derivatives and implied orthosilicate content is evident.

It is interesting to compare our inferred values of dK/dT and dG/dT, required of the β phase for consistency with the isochemical model mantle (Fig. 3), with those measured in the laboratory for other minerals (*22*); in general, data for silicates, oxides, and ionic solids imply that $|dG/dT|$ is less than $|dK/dT|$, whereas our solutions all require that $|dG/dT|$ is greater than $|dK/dT|$. Alternatively, we have also plotted in Fig. 3 the measured values of the parameters for mantle minerals given in table 1 of Duffy and Anderson [D&A (*16*)]. Although $|dG/dT|$ for olivine and garnet falls below the range of our inferred values, the data for the close-packed oxides of MgO and Al_2O_3 fall within or above this range. Thus, we conclude that the values of $|dG/dT|$ and $|dK/dT|$ inferred for an isochemical model mantle are not unreasonable in view of the available experimental data.

The results of earlier attempts to estimate these temperature derivatives (*15–18*) are also shown on Fig. 3. The values of Weidner and Ito (*18*) are not strictly comparable with the present calculations because their estimated pressure derivatives are not the same as the values we measured. The values estimated by Duffy and Anderson (*16*) and by Bina and Wood [B&W (*17*)], however, are most directly comparable because their estimated pressure derivatives agree within experimental error with those measured in this study. The analysis described above shows that the temperature derivatives estimated by these workers, applied to an isochemical model mantle, lead to calculated velocity contrasts with a ratio $\Delta V_P/\Delta V_S$ substantially different from unity (~0.8 for the values of D&A and ~1.3 for those of B&W), for which there is no compelling seismological evidence.

The value of the newly measured pressure derivatives has been illustrated by these calculations. However, definitive testing of the hypothesis whereby the 400-km discontinuity is the result of the olivine–β phase transformation in a model mantle of uniform composition must await the measurement of the temperature derivatives of the elastic moduli. For the same reason, no attempt has been made at this stage to model the velocity gradients within the transition zone.

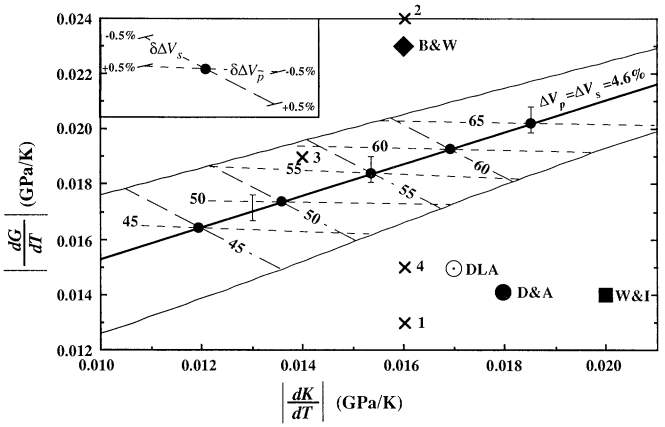

Fig. 3. Trade-off between $|dK/dT|$ and $|dG/dT|$ and the inferred composition (orthosilicate content) of a model mantle as discussed in the text. The heavy solid line represents calculations at a potential temperature of 1300°C with a seismic velocity contrast for both P and S waves of 4.6% at the 400 km discontinuity. Vertical bars show the effect of changing temperature by ±100°C. The outlying solid lines represent the effect of a ±0.5% change in ΔV_P or ΔV_S as indicated in the inset. Tie lines labeled with orthosilicate content (in percent) correspond to $(\delta\Delta V_P) = \pm 0.5\%$ at constant ΔV_S (lines with short dashes of slope ~0) and to $(\delta\Delta V_S) = \pm 0.5\%$ at constant ΔV_P (lines with long dashes of slope ~−3/4). Also shown are the measured values of these parameters for mantle minerals given in table 1 of Duffy and Anderson (*16*): 1, $(Mg,Fe)_2SiO_4$ olivine; 2, MgO; 3, Al_2O_3; 4, $Ca_3(Al,Fc)_2Si_3O_{12}$ garnet. Recent estimates of temperature derivatives are also shown on this figure: B&W, Bina and Wood (*17*); DLA, Anderson (*15*); D&A, Duffy and Anderson (*16*), W&I, Weidner and Ito (*18*).

REFERENCES AND NOTES

1. J. D. Bernal, *Observatory* **59**, 268 (1936); F. Birch, *J Geophys. Res.* **57**, 227 (1952).
2. Work of Ringwood's and other laboratories is summarized in A. E. Ringwood, *Composition and Petrology of the Earth's Mantle* (McGraw-Hill, New York, 1975).
3. D. L. Anderson, *Science* **157**, 1165 (1967).
4. T. Katsura and E. Ito, *J. Geophys Res.* **94**, 15663 (1989); M. Akaogi, E. Ito, A. Navrotsky, *ibid.*, p. 15671.
5. H. Sawamoto *et al.*, *Science* **224**, 749 (1984).
6. M. Kumazawa and O. L. Anderson *J. Geophys. Res.* **74**, 5961 (1969).
7. D. J. Weidner, *Geophys. Res. Lett.* **12**, 417 (1985); D. L. Anderson and J. D. Bass, *Nature* **320**, 321 (1986).
8. A solid-medium assembly was developed that attained pseudohydrostaticity in the split-sphere apparatus by surrounding the sample with NaCl. Under the synthesis conditions (P = 15 GPa, T = 1000°C), flow of NaCl results in the relaxation of deviatoric stresses. Careful control of the release path enabled recovery of samples in which internal strains had been annealed and no cracking or preferred orientation were observed even under the transmission electron microscope. Sample diameter

was 2.8 mm; length was 1.8 and 2.2 mm; and porosity (grain size <5 μm) was 0.4 and 0.8%, respectively, for the two samples. For each of the propagation directions, a pair of faces was ground and polished flat and parallel within 0.2 μm with 1-μm diamond paste. Details are in G. D. Gwanmesia, R. C. Liebermann, F. Guyot, *Geophys. Res. Lett.* **17**, 1331 (1990).
9. Phase comparison allows for accurate determination of elastic wave travel times over a wide frequency range. Dispersion attributable to departures at low frequencies from conditions of infinite-medium plane wave propagation is recognized. Its influence upon measured travel times is minimized by use of an average travel time for the high-frequency interval (50 to 70 MHz) over which travel time is relatively frequency-insensitive. For details see I. Jackson, H. Niesler, D. J. Weidner, *J. Geophys. Res.* **86**, 3736 (1981).
10. The interfaces between the acoustic buffer rod, a thin (2 μm thick) gold foil, and the specimen are loaded by the confining pressure in order to provide good mechanical coupling. Minor corrections are applied for the influence of this bond (~+1 ns in ~460 ns for P waves and ~−1.5 ns in 780 ns for S waves).
11. For detailed discussion of the high-pressure technique and pressure calibration see H. Niesler and I. Jackson, *J. Acoust. Soc. Am.* **86**, 1573 (1989); S. M. Rigden *et al.*, *Geophys. Res. Lett.* **15**, 605 (1988); H. Niesler, I. Jackson, E. C. Morris, *High Temp. High Pressures* **20**, 495 (1988).
12. R. K. Cook, *J. Acoust. Soc. Am.* **29**, 445 (1957).
13. Despite great care in polishing the ends of the specimens, the observed ratios of the buffer and sample echo amplitudes, and the low values of, and hysteresis among, the measured velocities indicate that the gold bond provides imperfect coupling between the buffer rod and specimen at pressures below ~1.4 GPa. See also (*11*).
14. Coefficients of Eulerian finite-strain Eqs. 1 and 2 are: $M_1 = G$; $L_1 = K + (4/3)G$; $M_2 = 5G - 3K(dG/dP)$; $M_2 = 5[K + (4/3)G] - 3K[dK/dP + (4/3)dG/dP]$.
15. D. L. Anderson, *J. Geophys. Res.* **93**, 4688 (1988).
16. T. S. Duffy and D. L. Anderson, *ibid.* **94**, 1895 (1989).
17. C. R. Bina and B. J. Wood, *ibid.* **92**, 4853 (1987).
18. D. J. Weidner and E. Ito, in *High-Pressure Research in Mineral Physics*, M. H. Manghnani and Y. Syono, Eds. (*Geophys. Monogr. Ser.*, vol. 39, American Geophysical Union, Washington, DC, 1987), pp. 239–446.
19. G. Nolet and M. J. R. Wortel in *Encyclopaedia of Geophysics*, D. A. James, Ed. (Van Nostrand Reinhold, New York, 1989), pp. 775–788.
20. S. P. Grand and D. V. Helmberger, *Geophys. J. R. Astron. Soc.* **76**, 399 (1984); L. V. Le Fevre and D. V. Helmberger, *J. Geophys. Res.* **94**, 17749 (1989).
21. D. McKenzie and M. J. Bickle, *J. Petrol.* **29**, 625 (1988) and references in (*3*).
22. Y. Sumino and O. L. Anderson, in *CRC Handbook of Physical Properties of Rocks*, R. S. Carmichael, Ed. (CRC Press, Boca Raton, FL, 1984), pp. 39–138.
23. We thank Z. Guziak for assistance with the ultrasonic measurements and the drafting of the illustrations. We thank B. L. N. Kennett, A. E. Ringwood, D. J. Weidner, T. Gasparik, A. L. Hales, T.-f. Wong, G. F. Davies, D. L. Anderson, and J. D. Bass for suggestions and comments. The High-Pressure Laboratory is supported by National Science Foundation (NSF) grants EAR 86-07105 and 89-17563 and the State University of New York at Stony Brook. This research was also supported by NSF grants EAR 88-17097 and the U.S.–Australia cooperative research program (NSF 1NT 8913363 and funding from the Australian Department of Industry, Technology and Commerce).

11 June 1990; accepted 30 July 1990

Methylation of an Immediate-Early Inducible Gene as a Mechanism for B Cell Tolerance Induction

VICKI L. SEYFERT, STEVEN B. MCMAHON, WILLIAM D. GLENN, AMY J. YELLEN, VIKAS P. SUKHATME, XINMIN CAO, JOHN G. MONROE*

Stage-specific gene regulation is important in determining cell function during development. Immature B cells expressing membrane-bound immunoglobulin M (mIgM) are sensitive to antigen-induced tolerance, whereas mature B cells are activated by antigen. Previous studies have established an association between *Egr-1* gene induction and antigen receptor (mIgM)–mediated activation of mature B cells. Here it is shown that the immature B cell line WEHI-231 and tolerance-sensitive bone marrow–derived B cells do not express *Egr-1*. It is further shown that lack of inducible expression in these cells is due to specific methylation of the *Egr-1* gene. Thus, covalent inactivation of an activation-associated gene may explain tolerance sensitivity at specific stages of B cell development.

THE DEVELOPMENTAL PROGRAM LEADING to mature murine B cells can be divided into windows defined by antigen receptor and phenotypic marker expression on the cell surface and by cellular responses of the B cells. Immature murine B cells express mIgM only, whereas mature murine B cells express both mIgM and membrane-bound immunoglobulin D (mIgD) (*1*). Recognition and binding of antigen to mIgM on mature murine B cells results in activation as defined by entry into the cell cycle (*2*) or competence for subsequent T cell–derived progression signals (*3*). In contrast, signaling through mIgM on immature murine B cells results in a negative response manifested by a state of induced unresponsiveness or tolerance (*4*). This phenomenon is believed to be responsible for the deletion or functional inactivation of those cells that recognize self-antigens.

Differential expression of growth-related genes may account, at least in part, for the different growth responses observed in immature versus mature B cells. This hypothesis is supported by studies of the expression of *Egr-1*, an immediate-early gene that encodes a transcriptional regulatory factor (*5, 6*). *Egr-1* is inducible in mature murine B cells (*7*) and in the phenotypically mature murine B cell line, BAL-17 (*8–10*), after mIgM is cross-linked with antibodies to IgM (anti-μ) or after stimulation with TPA (12-*O*-tetradecanoyl phorbol-13-acetate) (*7*). Induction by these signals is associated with a positive growth response (*7*). In contrast, *Egr-1* induction does not accompany anti-μ or TPA stimulation of the murine B cell line, WEHI-231 (*7, 10*), which possesses a stable immature B cell phenotype (*10–14*). Furthermore, this lack of *Egr-1* expression is associated with a negative growth response in these cells to mIgM-generated signals, which is manifested by an inhibition of proliferation leading to eventual cell death (*7, 13*). These results demonstrate an association between *Egr-1* gene expression and the transduction of mIgM signals into positive B cell growth responses.

To determine if a nontransformed population of cells analogous to WEHI-231 cells exists in vivo, we examined *Egr-1* expression in mIgM-positive ($mIgM^+$) cells from adult mouse bone marrow. Because these cells were of the immature phenotype ($mIgM^+$, $mIgD^-$) and did not manifest a positive activation response to signaling through mIgM (*15*), we reasoned that they belonged to the tolerance-sensitive B cell population previously defined (*4*). We observed no detectable induction of *Egr-1* expression in $mIgM^+$ cells in response to TPA stimulation (*16*) (Fig. 1, A and B). This result contrasts with that observed in mature splenic B cells (Fig. 1, C and D). Identical results were obtained after stimulation with anti-μ (*17*). Thus, a population of cells analogous to WEHI-231 cells exists in adult mouse bone marrow. Further molecular studies aimed at defining the causative factors responsible for the lack of inducible *Egr-1* expression in immature B cells were hindered by difficulties in maintaining the cells in culture and the heterogeneity inherent in primary cell populations. Thus, we used the WEHI-231 cell line as a model system for studying this stage of B cell development.

We considered the following as explanations for the inability of anti-μ or TPA to

V. L. Seyfert, S. B. McMahon, W. D. Glenn, A. J. Yellen, J. G. Monroe, Department of Pathology and Laboratory Medicine, University of Pennsylvania School of Medicine, Philadelphia, PA 19104–6084.
V. P. Sukhatme and X. Cao, Departments of Medicine and of Molecular Genetics and Cell Biology, Howard Hughes Medical Institute, University of Chicago, Chicago, IL 60637.

*To whom correspondence should be addressed.